Fuel 333 (2023) 126346

Contents lists available at ScienceDirect

Fuel

journal homepage: www.elsevier.com/locate/fuel

Full length article

Impact of alcohol–diesel fuel blends on soot primary particle size in a compression ignition engine

F.J. Martos [a,*], O. Doustdar [b], S. Zeraati-Rezaei [b], J.M. Herreros [b], A. Tsolakis [b]

[a] Escuela de Ingenierías Industriales, University of Málaga, c/Doctor Ortiz Ramos, s/n, 29071, Málaga, Spain
[b] Department of Mechanical Engineering, University of Birmingham, Edgbaston, B15 2TT, UK

ARTICLE INFO

Keywords:
Primary particle diameter
Soot
Compression ignition engines
Semi-empirical modelling
Alcoholic fuel blends

ABSTRACT

The use of alternative fuels, such as bio-alcohols, in advanced propulsion systems could a feasible strategy to address several of the current issues associated to the use of internal combustion engines fuelled by carbonaceous fossil fuels. Particularly, soot particles, are one of the key pollutants emitted from compression ignition engines. Therefore, the development of soot formation prediction models providing new understanding on the impact of alternative fuels combustion in compression ignition engines become essential for soot mitigation purposes.

This study proposes a new semi-empirical model that predicts in-cylinder soot primary particle growth from an engine fuelled with alcohol–diesel fuel blends. The model uses macroscopic experimental measurements of engine parameters such as instantaneous in-cylinder pressure. Furthermore, an empirical correlation is presented predicting the mean soot primary particle size as a function of alcohol–diesel fuel blend properties and fuel/air ratio. The experimental measurement of primary soot particle mean size are obtained from High Resolution Transmission Electron Microscope (HT-TEM) micrographs obtained from soot particles collected via thermophoresis. Overall, the research findings presented in this work contributes to propose environmentally friendly fuel candidates for transportation.

1. Introduction

Environmental and human health effects of pollutant emissions have resulted in increasingly stringent regulations as well as significant research efforts to decrease pollutant levels in the atmosphere [1]. Vehicles propelled by compression ignition engines have advantages in terms of lower fuel consumption and CO_2 emissions with respect to their counterpart spark ignition engines, while they present the challenge of the simultaneous reduction of particulate matter (PM) and NO_x emissions. Approaches which have been implemented to reduce global and local vehicular pollutant emissions include using alternative fuels, improving in-cylinder combustion and air management strategies and exhaust post-treatment technologies [2].

Alternative fuels have been proposed as a solution for vehicular propulsion systems to completely/partially replace conventional oil-derived. There are some key favourable characteristics such as their renewability, sustainability, lower carbon footprint, availability to supply the fuel demands and potential to reduce local and global pollutant emissions. Conventionally, biodiesel for compression ignition and bio-alcohols for spark-ignition engines are the most used alternative fuels. Bio-alcohols can be produced from lignocellulosic biomass using, for example, agricultural residue and switch grass. There are some advantages in the properties of alcohol fuels such as the high H/C ratio [3], absence of aromatic components, high oxygen-containing component (in this case, the hydroxyl group, OH) as well as excellent cold-flow properties [4]. These properties position them as good candidates for compression ignition engines, despite the apparent limitations due to their poor autoignition capabilities, lubricant properties and limited solubility within diesel in alcohol–diesel fuel blends [5]. Emissions reductions, especially in mass and number of particles, have been reported when individually blending methanol [6–8], ethanol [7–9], propanol [10] and butanol [7,8,11] with diesel fuel. The absence of aromatics, longer ignition delay and the presence of oxygen (O_2) in the alcohol fuel molecule have been reported as reasons for the observed particle reduction [9]. Results have also indicated that the presence of the OH group has a more significant particle reduction potential than that of the atomic oxygen within biodiesel [11].

The environmental and human health effects of particles do not only depend on the total mass and/or the number of emitted particles but also on particle size, morphology, and composition. For instance, smaller particles have larger surface/volume ratio are more reactive,

* Corresponding author.
E-mail address: fjmartos@uma.es (F.J. Martos).

https://doi.org/10.1016/j.fuel.2022.126346
Received 29 April 2022; Received in revised form 26 September 2022; Accepted 12 October 2022
Available online 1 November 2022

longer suspension residence time in the atmosphere and have higher deposition rates in the human respiratory system [12]. The shape of the particles emitted from compression ignition engines is chain-like composed of quasi-spherical primary particles [13,14]. Therefore, characteristics of the agglomerates such as shape, the number of primary particles, size of primary particles, and nano-structure are quantified to understand their formation, their potential effects on the environment and human health, as well as to provide guidelines for their abatement. Notably, the knowledge of primary particle size and the net growth rate of primary particles provide key information regarding in-cylinder formation process and particle reactivity. Also, primary particle size is a crucial input to feed models to determine soot agglomerates characteristics such as morphology and size as well as the greenhouse potential of particles [15,16]. Primary particle size distributions are commonly used to determine the number of primary particles per particle size. Primary particle size distributions are mathematically fitted to normal [17,18] and/or log-normal distribution functions [19], while other authors use an average primary particle size [20].

The effect of the engine operating condition on the primary particle size has been previously investigated. In-cylinder mass of fuel, partial pressure (concentration) of oxidant and temperature have been identified and included in models as critical parameters which control primary particles growth and oxidation [18,21]. Experimentally, the effect of in-cylinder temperature has been studied. There are some works which report that an increase in the in-cylinder temperature decreases primary particle size [22,23]. In contrast, other investigators have reported an increase in primary particle size [24–26] with the increase in temperature. The constant mean size of primary particles independently of the operating conditions, has been also reported [20,27]. Explanations provided are that an increase in the in-cylinder temperature produces a twofold effect by (i) increasing the rate of nucleation and surface growth, increasing primary particle size and (ii) enhancing soot oxidation, decreasing the primary particle size. The net effect on the primary particle size will depend on the compromise between the formation/growth and oxidation of primary particles, which would depend on the specific in-cylinder conditions such as temperature level [28], in-cylinder oxidant concentration, nature of particles, etc.

The effect of oxygenated fuel blends in carbonaceous primary particle size emitted from compression ignition engines has also been studied. Most investigations have been carried out with oxygenated fuels such as biodiesel and alcohol fuel blends. Generally, the average sizes of primary particles emitted from biodiesel combustion are lower than those emitted with conventional diesel fuel [29–31]. Regarding the effect of alcohol–diesel fuel blends, there is an agreement in the cited literature that the incorporation of butanol [32–35] and pentanol [36] into the fuel blends reduce the size of primary particles. Most of the literature agrees that the oxygen content of butanol reduces the inception of particle precursors and carbonaceous components involved in the growth of primary particles and enhances the rate of oxidation of the particles already formed.

This work develops a new semi-empirical model predicting the soot primary particle net growth (surface growth and oxidation) and the average net primary particle size of particles formed in compression ignition engines using conventional and alcohol–diesel fuel blends. The phenomenological soot primary particle net growth model is based on the Arrhenius equation incorporating key parameters including instantaneous in-cylinder pressure and temperature, the mass of fuel and air, as well as oxygen availability, which is distinguished between the oxygen provided by the intake air and the oxygen (in this case OH group) provided by the fuel. Butanol and pentanol have been chosen as non-cyclic long carbon chain alcohols due to their better blending stability, higher density, higher calorific value and higher cetane number compared to short-chain alcohols such as ethanol [10]. The effect of the inclusion of a cyclic group such as in the case of cyclopentanol has also been investigated. The outcomes of this investigation are supported by the already published literature which is limited to the effect of alcohol–diesel fuel blends on total engine output soot concentration [3,7,8,37] and average primary particle size [38].

Table 1
Test engine specifications [39].

Engine specification	Data
Number of cylinders	1
Bore	84 mm
Stroke	90 mm
Connecting rod length	160 mm
Compression ratio	16.1:1
Displacement volume	499 cm^3
Maximum injection pressure	1500 bar
Emissions' standard	designed for Euro 5

2. Methodology

2.1. Experimental setup

In this research, a four-stroke single-cylinder research diesel engine was used as shown in Fig. 1. The engine technical data and specifications are summarised in Table 1. The four-stroke diesel engine is naturally aspirated, water-cooled, equipped with exhaust gas recirculation (EGR) and common rail direct injection fuel system. An alternating current (AC) electric dynamometer was used to motor and load the engine. The engine was fuelled with diesel fuel, as a reference fuel and three other fuels blended with diesel. Butanol, pentanol and cyclopentanol were purchased from Sigma Aldrich. Their blends with diesel and neat diesel as the baseline fuel were tested to study the influence of various alternative fuels with different molecular structures. The alternative fuels were tested at a 20%v/v ratio with diesel fuel. The engine operating conditions are summarised in Table 2; 1500 rpm with 2 bar and 4 bar IMEP (Indicated Mean Effective Pressure) were selected as the engine rotational speed and load respectively, to reproduce low-load driving conditions. The common rail fuel injection pressure was set at 550 bar and 650 bar at 2 and 4 bar IMEP, respectively. The pilot fuel injection was set to start at 15° bTDC (before Top Dead Centre) with the duration of 0.150 ms; whereas the main injection started at 3° bTDC with the variable duration of around 0.443 ms to have a constant IMEP. In the studied cases, there is not any post fuel injection [39].

An AVL GH13P pressure transducer mounted in the cylinder head was used to record in-cylinder pressure, and an AVL FlexiFEM 2P2 amplifier amplified its signal. Also, a digital shaft encoder producing 360 pulses per revolution measured the crank–shaft position [40]. The pressure and crank–shaft position data was combined to create an in-cylinder pressure trace [39]. The temperatures at different points, such as on the exhaust manifold were recorded by using k-type thermocouples and a Pico Technology TC-08 thermocouple data logger. To monitor the air/fuel ratio in all tested conditions, an airflow meter was used to measure the engine intake air-flow. Then λ as a ratio of actual air/fuel ratio to stoichiometric air/fuel ratio was calculated and checked for all tested conditions [39].

An in-house developed LabVIEW programme connected to a National Instruments PCI-6023E data acquisition device was used to monitor and control the engine operating settings, such as injection pressure, timing and duration. To confirm combustion stability and minimise cyclic variability, the coefficient of variation (COV) of the IMEP for 200 cycles was monitored and it was < 4% for all of the test conditions. The LabVIEW programme analyses the engine indicated mean effective pressure for each cycle [39,41].

In-cylinder pressure data was pegged to have the same in-cylinder pressure at the bottom dead centre of the intake stroke as that of the intake manifold [42]. With logged average data of the in-cylinder pressure in 200 engine operating cycles, the heat release rate was obtained. Also, from the instantaneous mean in-cylinder pressure and by using a zero-dimensional thermodynamic model within the combustion chamber [43,44], the instantaneous mean temperature inside the combustion chamber can be obtained.

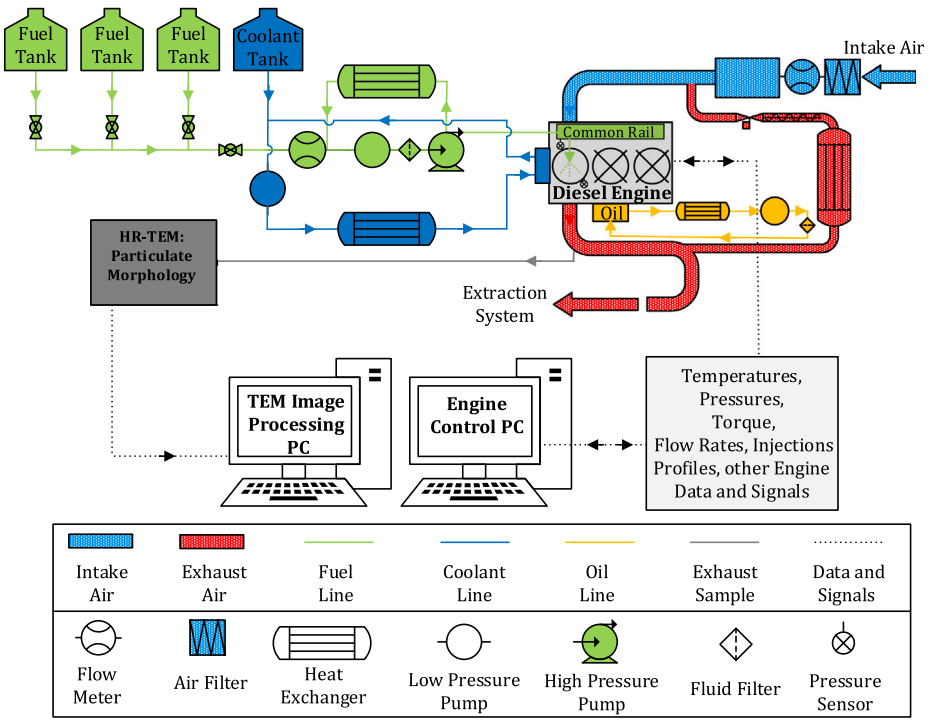

Fig. 1. Experimental set-up diagram.

Table 2
Engine test conditions abbreviations and colour codes.

Test abbreviation		Fuel blends with diesel (%v/v)	Engine speed (rpm)	Fuel injection pressure (bar)	IMEP (bar)	Injection timing bTDC-(CAD)	
						Pre	Main
D100L		Diesel 100%	1500	550	2	15	3
B20L		Butanol 20%	1500	550	2	15	3
P20L		Pentanol 20%	1500	550	2	15	3
CP20L		Cyclopentanol 20%	1500	550	2	15	3
D100M		Diesel 100%	1500	650	4	15	3
B20M		Butanol 20%	1500	650	4	15	3
P20M		Pentanol 20%	1500	650	4	15	3
CP20M		Cyclopentanol 20%	1500	650	4	15	3

Particle agglomerates were collected onto a formvar carbon film supported on a 3 mm diameter copper grid. A Talos^{TM} F200X S/TEM coupled to a FEI Ceta 16M^{TM} camera were utilised to obtain the high resolutions micrographs of particle agglomerates with a resolution up to 0.12 nm at a fast rate of 25 fps.

A bespoken digital image analysis software was utilised to measure 10 primary particles per agglomerate to a total of 30 agglomerates per fuel and engine operation condition. The conversion from pixels to nanometres was calibrated by comparison with standard latex spheres shadowed with gold.

Fig. 2.a shows a representative HR-TEM image from an agglomerate emitted from the combustion process of a fuel blend composed of 80% by volume of diesel and 20% of pentanol at low engine load. Fig. 2.b depicts how primary particles have been randomly selected from the agglomerate (marked with a red circle).

Fig. 3.a shows a typical agglomerate from the mid-load reference diesel engine tests, D100M. In the Figs. 3.b and 3.c two zones of the agglomerate are shown in which it can be appreciated how the growth is by graphite layers arranged as onion layers, tending to an almost spherical growth, as suggested by authors such as [45,46].

2.2. Fuels

The fuels used in this work are the reference diesel and three alcohol-type fuels, which are: butanol, pentanol and cyclopentanol. The main characteristics of neat fuels are shown in Table 3.

Alcohol fuels cannot be used in their neat state in conventional compression ignition engines, as they have poor autoignition properties. So, they were blended with the reference fuel in the proportion of 20% by volume of alcoholic fuel and 80% by volume of reference fuel. The mixture between diesel and butanol has been called B20, between diesel and pentanol has been called P20, and finally, between diesel and cyclopentanol has been called CP20. Relevant physicochemical characteristics of the studied fuel blends are shown in Table 4.

2.3. Model

There is not a single primary particle size within the same agglomerate (Figs. 2 and 3) as the size depends on multiple factors including fuel spatial distribution, local thermodynamic and mixing conditions around fuel spray formation, local dehydrogenation of the fuel, etc. It is therefore proposed to develop a growth model for the average primary particle size.

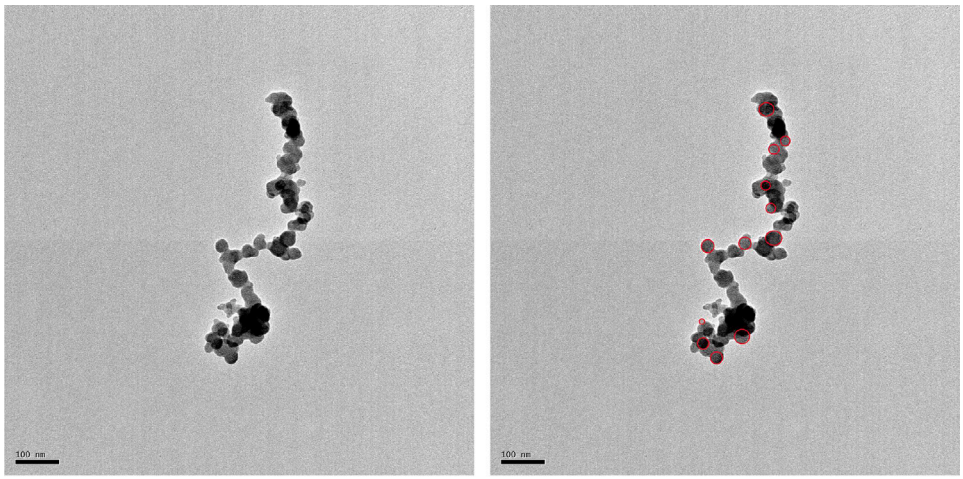

Fig. 2. Soot agglomerate from P20L tests (a) No primary particles indicated, (b) Primary particles indicated. (For interpretation of the references to colour in this figure legend, the reader is referred to the web version of this article.)

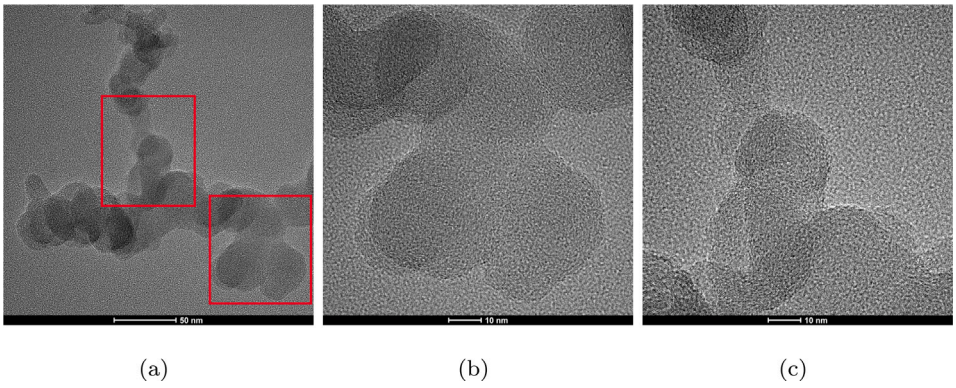

Fig. 3. Soot agglomerate from tests D100M.

A growth model based on the Hiroyasu–Nagle and Strickland model is proposed, in which there are a formation term and a reduction or disappearance term for the carbon layers [48]. Furthermore, it is assumed that both the growth and the reduction of the primary particles are made by means of thin spherical layers [18]. Eq. (1) shows that the instantaneous net growth of the outer surface of a mean primary particle, $\overline{S_{net}}$, is the balance between the instantaneous surface growth/formation, $\overline{S_f}$, by the effect of fuel dehydrogenation and subsequent precursor formation [49], and the instantaneous reduction of the outer surface by oxidation, $\overline{S_{ox}}$, [50].

$$\frac{\mathrm{d}\overline{S_{net}}}{\mathrm{d}t} = \frac{\mathrm{d}\overline{S_f}}{\mathrm{d}t} - \frac{\mathrm{d}\overline{S_{ox}}}{\mathrm{d}t} \tag{1}$$

The term soot formation mainly depends on the in-cylinder pressure and temperature [51]. Soot formation is modelled by an Arrhenius type expression where the pre-exponential term is dependent on the instantaneous mean in-cylinder pressure, $p(t)$, and the exponential term depends on instantaneous mean in-cylinder temperature, $T(t)$, as is shown in Eq. (2).

$$\frac{\mathrm{d}\overline{S_f}}{\mathrm{d}t} = A_f\, p(t)^{B_f} \exp\left(-\frac{E_f}{R\,T(t)}\right) \tag{2}$$

In Eq. (2) A_f and B_f are two constants, R is the gas constant and E_f is the activation energy of soot formation. In this case, the term E_f/R has been taken from the Refs. [52,53] and is equal to 12100 K.

The soot oxidation and formation terms depend on the in-cylinder pressure [51], and temperature and it is also modelled by an Arrhenius expression [52]. In this case, a modified Arrhenius type expression will be used depending on the instantaneous mean pressure within the combustion chamber. Three more terms have been introduced: (i) one dependent on the instantaneous mean oxygen mass fraction within the combustion chamber, $Y(t)_{\mathrm{O}_2,ox}$, (ii) another dependent on the instantaneous hydroxyl radical mass fraction of the fuel, $Y(t)_{\mathrm{OH},fuel}$, which must have a significant oxidising effect, (iii) a term that depends proportionally on the size of the particle to consider the larger outer surface of large particles. The soot oxidation term is shown in Eq. (3).

$$\frac{\mathrm{d}\overline{S_{ox}}}{\mathrm{d}t} = A_{ox}\, p(t)^{B_{ox}} \left(1 + C_{ox} Y(t)_{\mathrm{OH},fuel}\right) Y(t)_{\mathrm{O}_2,ox}^{D_{ox}} \exp\left(-\frac{E_{ox}}{RT(t)}\right) \overline{S_{net}}^{F} \tag{3}$$

In Eq. (3) the coefficients A_{ox}, B_{ox}, C_{ox} and D_{ox} are constant. The variable E_{ox} is the soot oxidation activation energy. In this case the term E_{ox}/R has been taken from the Refs. [52,53] and is equal to 19680 K. The order of soot reaction as solid-state is 0.5, [54,55], so the constant F has been taken equal to 0.5.

The equation to be solved is obtained by replacing the Eqs. (2) and (3) in Eq. (1). All time-dependent terms in Eq. (2) have been included in the $f(t)$ function, and equally, all time-dependent terms in Eq. (3) are grouped in the $g(t)$ function. In addition, the mean surface area of the primary particle, $\overline{S_{net}}$, has been replaced by its diameter, $\overline{d_{po}}$. The Eq. (4) models the temporal evolution of the mean diameter of the primary particle.

$$\frac{\mathrm{d}\overline{d_{po}}}{\mathrm{d}t} = \frac{2}{\pi} f(t) - \frac{1}{\sqrt{\pi}} g(t) \overline{d_{po}} \tag{4}$$

Table 3
Main properties of net fuels [47].

Property	Diesel	Butanol	Pentanol	Cyclopentanol
Molecular formula	$\sim C_{12}H_{22}$	C_4H_9OH	$C_5H_{11}OH$	C_5H_9OH
Molecular weight (g mol^{-1})	166.3	74.11	88.15	86.13
Purity (%, v/v)	–	99	99	99
Density at 15 °C (kg m^{-3})[a]	834.8	811.5	814.8	949
Viscosity at 40 °C (cSt)[b]	2.63	2.17	2.74	2.84
Lower heating value (MJ kg^{-1})[c]	45.97	33.81	34.65	35.96
Heat of evaporation (kJ kg^{-1})	270–350	581.4	308.1	–
Lubricity at 60 °C (μm)[d]	463	628	579	452
Surface tension at 25 °C (mN m^{-1})[e]	26.07	23.05	24.02	31.35
Cetane number[f]	53.0	15.9	18.2	9.8
H/C ratio	1.8	2.5	2.4	2.0
$(Fuel/Air)_{sth}$ ratio	1/14.48	1/11.14	1/11.71	1/11.18
Carbon (%w/w)	86.44	64.87	68.18	69.76
Hydrogen (%w/w)	13.56	12.16	12.50	10.47
Hydroxyl radical (%w/w)	0	22.97	19.32	19.77
CFPP (° C)[g]	−20.0	−41.7	−47.0	−47.1
Water content (mg kg^{-1})[h]	41.7	11.5	29.7	–
Boiling point (° C)	180–360	117.4	137.9	140.4
Cloud point (° C)[i]	−4.1	−115.5	–	–
Pour point (° C)[j]	−21	<-120.7	–	–
Flash point (° C)	68	35	49	51

[a]Method: EN ISO 3675.
[b]Method: EN ISO 3104.
[c]Method: ASTM D240–02.
[d]Method: EN ISO 12156–1.
[e]Method: ASTM D971.
[f]Method: ASTM D6890.
[g]Method: EN 116.
[h]Method: EN ISO 12937.
[i]Method: EN 23015.
[j]Method: ASTM D97.

Table 4
Main properties of fuel blends.

Property	B20	P20	CP20
Density at 15 °C (kg m^{-3})[a]	830.1	830.8	857.6
Viscosity at 40 °C (cSt)[b]	2.27	2.60	2.75
Lower heating value (MJ kg^{-1})[c]	43.54	43.99	43.97
Lubricity (μm)[d]	570	562	480
Surface tension at 25 °C (mN m^{-1})	25.48	24.78	26.30
$(Fuel/Air)_{sth}$ ratio	1/13.83	1/13.94	1/13.75
Carbon (%w/w)	82.47	83.10	82.99
Hydrogen (%w/w)	13.04	13.11	12.64
Hydroxyl radical (%w/w)	4.49	3.79	4.37
CFPP (° C)[e]	−19.99	−20.06	−20.07

[a]Method: EN ISO 3675.
[b]Method: EN ISO 3104.
[c]Method: ASTM D240-02.
[d]Method: EN ISO 12156–1.
[e]Method: EN–116.

The Eq. (4) is an ordinary first-order differential equation, the general solution of which can be obtained from [56] and is:

$$\overline{d_{po}}(t) = exp\left(-\int \frac{1}{\sqrt{\pi}} g(t)\mathrm{d}t\right)\left[\int \frac{2}{\pi} f(t)\cdot exp\left(\int \frac{1}{\sqrt{\pi}} g(t)\mathrm{d}t\right)\mathrm{d}t + C\right] \tag{5}$$

In Eq. (5), C is the integration constant.

In Eq. (3), the term temporary mass fraction of oxygen within the combustion chamber has been modelled according to [57]. In this case, the exhaust gas recirculation and the gas escaping into the crankcase are assumed to be zero, so that the temporary oxygen mass fraction within the combustion chamber is:

$$Y(t)_{O_2,ox} = Y_{O_2,air}\left(1 - \phi\, HRF(t)\right) \tag{6}$$

In Eq. (6), the term $Y_{O_2,air}$ is the mass fraction of oxygen in the air and is approximately equal to 0.23. $HRF(t)$ is the time-dependent accumulated heat release fraction and ϕ is the equivalence ratio.

And finally, in Eq. (3), the term temporary mass fraction of the hydroxyl radical released from the fuel inside the combustion chamber has been modelled as a function of the heat release rate.

$$Y(t)_{OH,fuel} = Y(t=0)_{OH,fuel}\left(\frac{(F/A)}{1+(F/A)}\right)\left(1 - HRF(t)\right) \tag{7}$$

In Eq. (7), the term $Y(t=0)_{OH,fuel}$ is the mass fraction of the hydroxyl radical in the fuel and (F/A) is the fuel/air ratio.

3. Results and discussion

3.1. Test results

3.1.1. Engine operating conditions

Table 5 shows the average fuel and air consumption, maximum in-cylinder pressure and equivalence ratio, ϕ, for all the fuels at each engine operation condition, where engine speed and engine load are equal for all the fuels.

It can be seen in Table 5 that the fuel with the lowest absolute consumption is diesel, and this is due to its higher calorific value, as long as the same degree of load and engine speed is maintained, as is the case here. There is no clear trend for other fuel mixtures.

3.1.2. Mean in-cylinder pressure

The instantaneous in-cylinder pressure is shown in Fig. 4.a for low load (IMEP∼ 2 bar) and in Fig. 4.b for medium load (IMEP∼ 4 bar) engine operation. The starting point for the model has been located when the combustion starts for each fuel.

Fig. 4.a and 4.b show how the evolution of in-cylinder pressure follow a similar pattern characteristic of conventional combustion for all the studied fuels. Generally, the combustion of the alcohol–diesel fuel blends produces a higher maximum in-cylinder pressure with

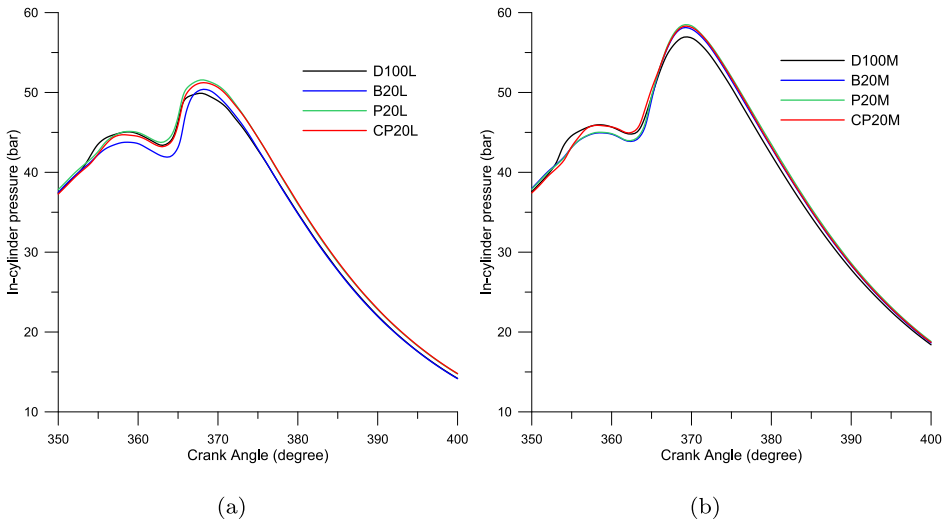

Fig. 4. Average pressure inside the combustion chamber vs. crank angle degree. (a) Low load Modes, *L*, (b) Medium load Modes, *M*.

Table 5
Engine operating conditions.

Operating mode	Fuel (kg/h)	Air (kg/h)	p_{max} (bar)	ϕ
D100L	0.366	17.42	49.90	0.3041
B20L	0.407	17.05	50.37	0.3299
P20L	0.414	17.42	51.58	0.3310
CP20L	0.434	17.35	51.22	0.3438
D100M	0.649	17.27	56.92	0.5439
B20M	0.659	17.42	58.11	0.5228
P20M	0.678	17.13	58.46	0.5513
CP20M	0.668	17.13	58.28	0.5359

respect to the maximum in-cylinder pressure resulting from diesel fuel combustion for each engine operation load. This is well supported by the lower autoignition tendency of the alcohol fuel which slightly delays the start of combustion increasing the quantity of fuel burnt in premixed combustion phase and thus the maximum in-cylinder pressure [11].

Fig. 5 shows as a representative example, from the results derived from the combustion process of the butanol–diesel fuel blend for both engine operation conditions. Instantaneous mean in-cylinder pressure (black), rate of heat release (green), in-cylinder oxygen fraction due to the air (red) calculated using Eq. (6) and mass fraction of the hydroxyl radical (blue) calculated using Eq. (7) are shown in Fig. 5. Similar patterns are obtained for the rest of fuel blends, but are not shown for the clarity of the results. The main difference between the fuels is the mass fraction of the hydroxyl radical.

Comparing Fig. 5.a with 5.b shows how an increase in the final oxygen mass fraction in the chamber is obtained with the decrease of engine load.

3.1.3. Measured primary particles

A minimum of 30 photographs obtained in HR-TEM have been taken as the image shown in Fig. 2 of each engine operating mode and for each fuel. For each photograph a minimum of 10 primary particles has been measured, so that for each engine operating mode and for each fuel tested, there is a population of no less than 300 primary particles. The histogram shown in Fig. 6 has been obtained from this population.

All samples were subjected to the nonparametric Kolmogórov–Smirnov normality test enhanced with the Lilliefors test. In all cases, the distribution obtained is normal, as shown in Fig. 6.

The average size of primary particles formed during the combustion process of alcohol–diesel fuel blends is always smaller than the size of those emitted under diesel fuel combustion for the two studied engine loads. It is thought that the higher H/C ratio, the longer the ignition delay and the presence of fuel-borne oxygen (in this case OH) contribute to this result, as it has been previously reported in [32–36,38].

In Fig. 6 it is observed that with the increase of engine load, there is a greater dispersion of the sizes of the primary particles when the engine works with the mixtures of alcoholic fuels. In the case of an engine operating on pure diesel, the dispersion of the primary particle sizes does not change significantly. This effect may be because the mass increase of alcoholic fuel within the combustion chamber can significantly change the local conditions in which soot precursors are produced, causing both small and large soot particles to be generated in similar proportions.

Also, in Fig. 6, it is observed that the greater the engine load, the greater the average diameter of the primary particles for all fuels. This effect may be because the greater the engine load, the greater the fuel/air ratio, and the greater the mass of fuel injected, thus increasing the likelihood of generating new soot precursors [58]. This is also supported by the fact that an increase in the in-cylinder temperature promotes primary particle growth more than particle oxidation, as it has been reported for low-temperature levels, as in this case (low and medium load conditions) [28].

From the data shown in the Tables 3–5 a multiparametric correlation has been obtained with a very high adjustment coefficient, $R^2 = 0.960$. So, there is an almost linear relationship between the mean diameter of the primary particles and the independent variables shown in Eq. (8).

$$\overline{d_{po}} = 984.226 - 11.255\, Y_{\mathrm{OH},fuel} - 15.982\, H_p - 16.360\, Y_{\mathrm{H},fuel} - 0.147\, \frac{A}{F} \quad (8)$$

In the correlation shown in Eq. (8) the appearance of independent variables have been ordered according to which effect is more predominant, $Y_{\mathrm{OH},fuel}$, or less predominant, (A/F), on the mean diameter of the primary particles.

So, the larger the mass fraction of hydroxyl group in the fuel, the greater the probability that the mean diameter of the primary particles will be smaller. This may be due to the lower probability of generating precursors due to the oxidising effect of the hydroxyl radical. The greater the heating value of the fuel, the smaller quantity of fuel injected to maintain the same load (particularly for this study as indicated/brake thermal efficiency is similar for all fuels) and the greater the average temperature in the combustion chamber both reducing particle formation in the studied conditions [50]. The lower the hydrogen content in the fuel the greater the probability of generating larger primary particles. This may be because the lower the mass of hydrogen in the fuel the less energy there is to dehydrogenate the fuel

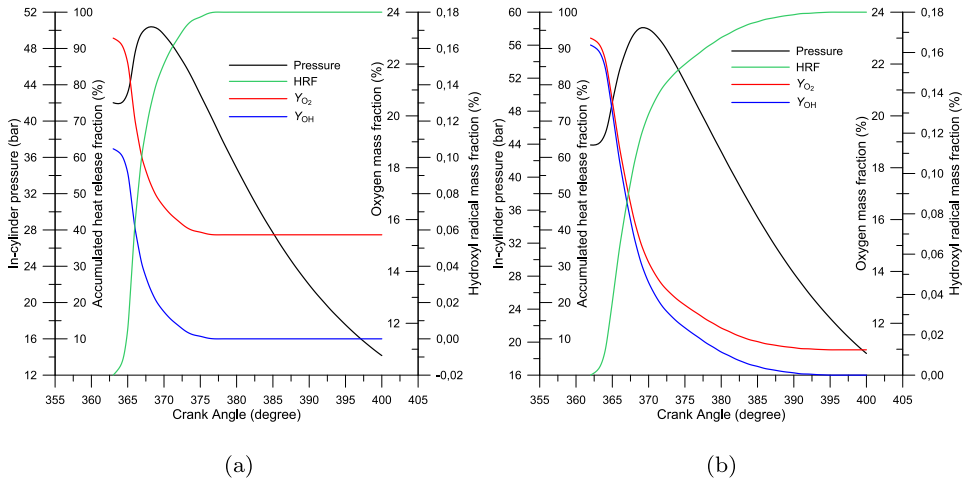

Fig. 5. Time evolution of pressure, HRF, Y_{O_2} and Y_{OH} vs. crank angle degree. (a) B20L, (b) B20M.

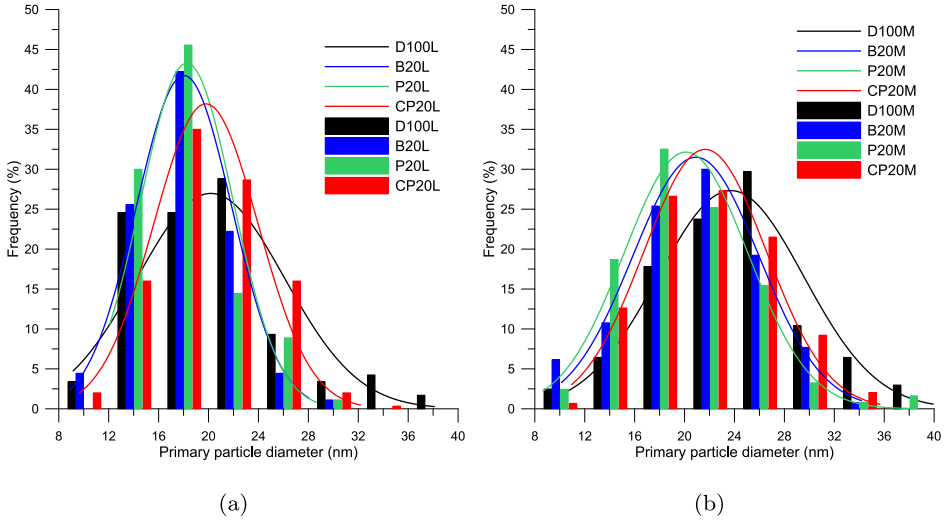

Fig. 6. Histograms of mean diameters of primary particles measured experimentally. (a) Low load Modes, L, (b) Medium load Modes, M.

and the greater the likelihood of soot precursor generation. As for the effect of the air/fuel mass ratio is the least significant of all, so the greater the mass of fuel injected or the smaller the mass of air introduced into the combustion chamber, the greater is the probability of generating new graphite layers, producing soot precursors and carbon components and therefore greater will be the average diameter of the primary particles [25].

3.2. Application of the model

The model coefficients have been obtained, minimising the mean quadratic error between modelled primary particle size obtained by Eq. (1) and average experimental primary particle size shown in Fig. 6. In this case, a minimum mean quadratic error of 0.3210 has been obtained for the coefficients: $A_f = 509366$, $A_{ox} = 19731$, $B_f = 2.667$, $B_{ox} = 4.429$, $C_{ox} = 9869$ y $D_{ox} = -0.046$. For other engine size configurations, injector and combustion chamber geometry, engine operating conditions such as engine speed, load, EGR, etc., these coefficients must be re-fitted.

Fig. 7 depicts the temporal evolution of mean size of primary particles applying the model shown in Eq. (5) using the optimised constant values for the fitting parameters (represented by a thick continuous line in the plot). The net rate of primary particle size growth/oxidation has also been obtained by calculating the temporal derivate, shown as thin continuous lines in Fig. 7.

Fig. 7.a shows the primary particles results for low load engine operation, while Fig. 7.b shows the results for engine medium load. In all cases, the time derivative of the diameter terminates in zero for crank angles above 440°, meaning that the primary particles do not evolve from that point. It should be noted that when combustion begins, the growth rate of the primary particles for the case of 100% diesel, D100, is very high, until the average temperature rises and the reduction of the graphite layers on the periphery of the soot are oxidised. This effect is best seen in Fig. 7.b which corresponds to the case of D100M, at medium load, in which the thermal effect is seen as predominant from about 367 °CAD, in which the rate of decrease is in the order of the preliminary growth rate. From there, the growth of the primary particles is sustained with a relatively low growth rate and decreases until becoming zero.

For alcohol–diesel fuel blends, it can be observed that the growth of primary particles is suppressed by oxidation of the hydroxyl radical in the first stages of the formation of the graphene layers. This effect is best appreciated in medium load conditions, Fig. 7.b, in which the delay in forming primary particles with diameters of 1 nm on average reaches 370 °CAD. From these CAD angles, the growth rate of soot formed when the engine operates on alcohol–diesel fuel blends is higher than when the fuel is pure diesel, and this may be because, for the same

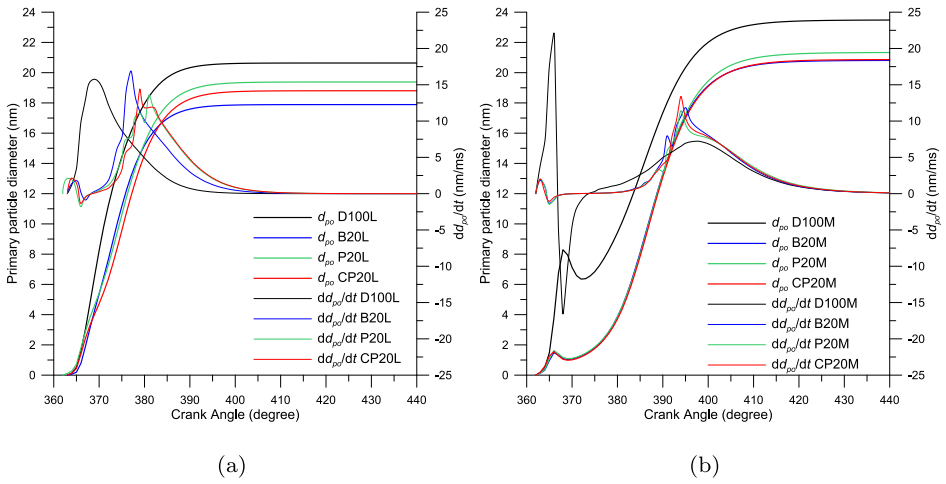

Fig. 7. Temporal evolutions of the mean diameter of the primary particles and their temporal derivative vs. crank angle degree.

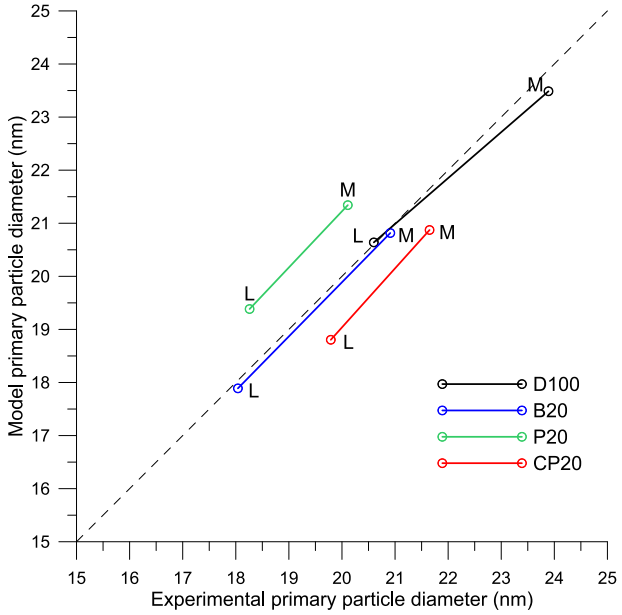

Fig. 8. Mean diameters of the primary particles obtained by the proposed model vs. the experimental ones.

CAD angles, the primary soot particles are much smaller for alcohol–diesel fuel blends and therefore fewer soot precursors are needed to form the same graphite layers as the pure diesel engine, since the surface area of the primary particles is smaller.

In Fig. 8 is shown the mean diameters of the primary particles measured experimentally versus those obtained by the model shown in Fig. 7.

Fig. 8 represents the modelled concerning the experimental primary particle sizes. It can be seen that all results are close to the bisecting line, represented by a dashed line in the figure.

4. Conclusions

The size of the primary particles generated by a compression ignition engine running at low and medium loads with four different fuels has been measured experimentally. Pure diesel and three fuel blends composed of 80% diesel (by volume) with 20% of butanol, pentanol and cyclopentanol have been investigated. Based on these experimental measures and the physical and chemical characteristics of the fuels, a correlation has been obtained that predicts accurately the average diameter of the primary particles emitted, which depends mainly (in decreasing order of their effect) on the mass fraction of the hydroxyl group in the fuel, on the mass fraction of hydrogen in the fuel and on the air/fuel ratio. In all cases, the larger any of these variables, the smaller the average primary particle diameter.

A new semi-empirical model has been developed predicting the instantaneous soot primary particle net growth, and thus, average primary particle size depending on engine condition and fuel properties. For alcohol–diesel blends, it can be observed that the growth of primary particles is suppressed by oxidation of the hydroxyl radical in the first stages of forming the graphene layers. The model is based on the mean in-cylinder pressure and temperature and fuel oxygen content as major inputs and geometric engine characteristics such as engine displacement, stroke, piston diameter and compression ratio. The model can reproduce the smaller primary particle size for diesel–alcohol blends concerning diesel fuel combustion and the larger primary particle size of medium load concerning low load engine operation. This investigation provides new knowledge and tools which contribute to propose environmentally friendly fuel candidates for transportation.

CRediT authorship contribution statement

F.J. Martos: Conceptualisation, Methodology, Formal analysis, Investigation, Supervision, Writing – original draft, Writing – review & editing. **O. Doustdar:** Investigation, Formal analysis, Writing – original draft. **S. Zeraati-Rezaei:** Investigation, Formal analysis, Writing – original draft. **J.M. Herreros:** Investigation, Resources. **A. Tsolakis:** Project administration, Conceptualization, Methodology, Funding acquisition, Supervision, Writing – review & editing.

Declaration of competing interest

The authors declare that they have no known competing financial interests or personal relationships that could have appeared to influence the work reported in this paper.

Data availability

Data will be made available on request.

Acknowledgements

F.J. Martos expresses thanks (1) the government of Spain for supporting his research stay with reference PRX19/00187 at University of Birmingham and (2) the University of Malaga for supporting through the supercomputing and Bioinnovation Center and in particular to

the supercomputer Picasso belonging to the Spanish Supercomputing Network. ESPRC is acknowledged for supporting this work with the project FACE (ESPRC: ref. EP/P03117X/1).

Appendix. Nomenclature

A	air
A	constant
B	constant
C	constant
C	carbon
d	diameter
D	constant
E	activation energy
f	function
F	constant
F	fuel
g	function
H	hydrogen
H_p	lower heating value
HRF	accumulated heat release fraction
L	low
M	medium
p	pressure
O_2	oxygen
R	gas constant
S	surface
t	time
T	temperature
v	volume
w	weight
Y	mass fraction
λ	inverse equivalence ratio
ϕ	equivalence ratio

Subscripts

air	air
f	formation
$fuel$	fuel
H	hydrogen
max	maximum
net	net
po	primary particle
O_2	oxygen
OH	hydroxyl group
ox	oxidation
po	primary particle
sth	stoichiometric

Acronyms

AC	Alternating current
bTDC	Before top dead centre
CAD	Crank angle degree
COV	Coefficient of variation
EGR	Exhaust gas recirculation
HR-TEM	High resolution transmission electronic microscopy
IMEP	Indicated mean effective pressure
PM	Particulate matter

References

[1] 2008/692/EC, Implementing and amending Regulation (EC) No 7152007 of the European Parliament and of the Council on type-approval of motor vehicles with respect to emissions from light passenger and commercial vehicles (Euro 5 and Euro 6) and on access to vehicle repair and maintenance information.

[2] Tsolakis A, Bogarra M, Herreros JM. Chapter 1: Road Vehicle Technologies and Fuels. Issues in Environmental Science and Technology No. 44. In: Hester RE, Harrison RM, editors. Environmental impacts of road vehicles: Past, present and future. The Royal Society of Chemistry; 2017, p. 1–24.

[3] Tutak W, Lukacs K, Szwaja S, Bereczky A. Alcohol–diesel fuel combustion in the compression ignition engine. Fuel 2015;154:196–206. http://dx.doi.org/10.1016/j.fuel.2015.03.071.

[4] Lapuerta M, Rodríguez-Fernández J, Fernández-Rodríguez D, Patiño-Camino R. Cold flow and filterability properties of n-butanol and ethanol blends with diesel and biodiesel fuels. Fuel 2018;224:552–9. http://dx.doi.org/10.1016/j.fuel.2018.03.083.

[5] Lapuerta M, García-Contreras R, Campos-Fernández J, Dorado MP. Stability, lubricity, viscosity, and cold-flow properties of alcohol-diesel blends. Energy & Fuels 2010;24(8):4497–502. http://dx.doi.org/10.1021/ef100498u.

[6] Cheung C, Zhu L, Huang Z. Regulated and unregulated emissions from a diesel engine fueled with biodiesel and biodiesel blended with methanol. Atmos Environ 2009;43(32):4865–72. http://dx.doi.org/10.1016/j.atmosenv.2009.07.021.

[7] Kumar V, Singh AP, Agarwal AK. Gaseous emissions (regulated and unregulated) and particulate characteristics of a medium-duty CRDI transportation diesel engine fueled with diesel-alcohol blends. Fuel 2020;278:118269. http://dx.doi.org/10.1016/j.fuel.2020.118269.

[8] Ning L, Duan Q, Chen Z, Kou H, Liu B, Yang B, et al. A comparative study on the combustion and emissions of a non-road common rail diesel engine fueled with primary alcohol fuels (methanol, ethanol, and n-butanol)/diesel dual fuel. Fuel 2020;266:117034. http://dx.doi.org/10.1016/j.fuel.2020.117034.

[9] Lapuerta M, Armas O, Herreros JM. Emissions from a diesel–bioethanol blend in an automotive diesel engine. Fuel 2008;87(1):25–31. http://dx.doi.org/10.1016/j.fuel.2007.04.007.

[10] Kumar BR, Saravanan S. Use of higher alcohol biofuels in diesel engines: A review. Renew Sustain Energy Rev 2016;60:84–115. http://dx.doi.org/10.1016/j.rser.2016.01.085.

[11] Sukjit E, Herreros JM, Piaszyk J, Dearn K, Tsolakis A. Finding synergies in fuels properties for the design of renewable fuels–hydroxylated biodiesel effects on butanol-diesel blends. Environ Sci Technol 2013;47(7):3535–42. http://dx.doi.org/10.1021/es400131j.

[12] Soderholm SC. Proposed international conventions for particle size-selective sampling. Ann Occup Hyg 1989;33(3):301–20. http://dx.doi.org/10.1093/annhyg/33.3.301.

[13] Bonczyk PA, Hall RJ. Fractal properties of soot agglomerates. Langmuir 1991;7(6):1274–80. http://dx.doi.org/10.1021/la00054a042.

[14] Hwang J, Hirner FS, Bae C, Patel C, Gupta T, Agarwal AK. HRTEM evaluation of primary soot particles originated in a small-bore biofuel compression-ignition engine. Appl Therm Eng 2019;159:113899. http://dx.doi.org/10.1016/j.applthermaleng.2019.113899.

[15] Dobbins RA, Megaridis CM. Absorption and scattering of light by polydisperse aggregates. Appl Opt 1991;30(33):4747–54. http://dx.doi.org/10.1364/AO.30.004747.

[16] Charalampopoulos TT, Shu G. Effects of polydispersity of chainlike aggregates on light-scattering properties and data inversion. Appl Opt 2002;41(4):723–33. http://dx.doi.org/10.1364/AO.41.000723.

[17] Park K, Kittelson DB, McMurry PH. Structural properties of diesel exhaust particles measured by transmission electron microscopy (TEM): Relationships to particle mass and mobility. Aerosol Sci Technol 2004;38(9):881–9. http://dx.doi.org/10.1080/027868290505189.

[18] Lapuerta M, Martos FJ, Herreros JM. Effect of engine operating conditions on the size of primary particles composing diesel soot agglomerates. J Aerosol Sci 2007;38(4):455–66. http://dx.doi.org/10.1016/j.jaerosci.2007.02.001.

[19] Ryser R, Gerber T, Dreier T. Soot particle sizing during high-pressure Diesel spray combustion via time–resolved laser–induced incandescence. Combust Flame 2009;156(1):120–9. http://dx.doi.org/10.1016/j.combustflame.2008.08.005.

[20] Müller J-O, Su DS, Jentoft RE, Wild U, Schlögl R. Diesel engine exhaust emission: oxidative behavior and microstructure of black smoke soot particulate. Environ Sci Technol 2006;40(4):1231–6. http://dx.doi.org/10.1021/es0512069.

[21] Martos F, Martín-González G, Herreros J. Semi-empirical model for indirect measurement of soot size distributions in compression ignition engines. Measurement 2018;124:32–9. http://dx.doi.org/10.1016/j.measurement.2018.03.081.

[22] Mathis U, Mohr M, Kaegi R, Bertola A, Boulouchos K. Influence of diesel engine combustion parameters on primary soot particle diameter. Environ Sci Technol 2005;39(6):1887–92. http://dx.doi.org/10.1021/es049578p.

[23] Lee KO, Cole R, Sekar R, Choi MY, Zhu J, Kang J, et al. Detailed characterization of morphology and dimensions of diesel particulates via thermophoretic sampling. Tech. rep., SAE Technical Paper; 2001, http://dx.doi.org/10.4271/2001-01-3572.

[24] Neer A, Koylu UO. Effect of operating conditions on the size, morphology, and concentration of submicrometer particulates emitted from a diesel engine. Combust Flame 2006;146(1–2):142–54. http://dx.doi.org/10.1016/j.combustflame.2006.04.003.

[25] Crookes RJ, Sivalingam G, Nazha MA, Rajakaruna H. Prediction and measurement of soot particulate formation in a confined diesel fuel spray-flame at 2.1 MPa. Int J Therm Sci 2003;42(7):639–46. http://dx.doi.org/10.1016/S1290-0729(03)00029-2.

[26] Arai M, Amagai K, Nakaji T, Hayashi S. Primary and aggregate size distributions of PM in tail pipe emissions form diesel engines. JSME Int J 2005;48(4):639–47. http://dx.doi.org/10.1299/jsmeb.48.639.

[27] Lehtinen KE, Zachariah MR. Energy accumulation in nanoparticle collision and coalescence processes. J Aerosol Sci 2002;33(2):357–68. http://dx.doi.org/10.1016/S0021-8502(01)00177-X.

[28] Zhu J, Lee KO, Yozgatligil A, Choi MY. Effects of engine operating conditions on morphology, microstructure, and fractal geometry of light-duty diesel engine particulates. Proc Combust Inst 2005;30(2):2781–9. http://dx.doi.org/10.1016/j.proci.2004.08.232.

[29] Liati A, Spiteri A, Eggenschwiler PD, Vogel-Schäuble N. Microscopic investigation of soot and ash particulate matter derived from biofuel and diesel: implications for the reactivity of soot. J. Nanoparticle Res 2012;14(11):1224. http://dx.doi.org/10.1007/s11051-012-1224-7.

[30] Ma Y, Zhu M, Zhang Z, Zhang D. Effect of a homogeneous combustion catalyst on the nanostructure and oxidative properties of soot from biodiesel combustion in a compression ignition engine. Proc Combust Inst 2015;35(2):1947–54. http://dx.doi.org/10.1016/j.proci.2014.06.008.

[31] Savic N, Rahman M, Miljevic B, Saathoff H, Naumann K, Leisner T, et al. Influence of biodiesel fuel composition on the morphology and microstructure of particles emitted from diesel engines. Carbon 2016;104:179–89. http://dx.doi.org/10.1016/j.carbon.2016.03.061.

[32] Lapuerta M, Oliva F, Agudelo JR, Boehman AL. Effect of fuel on the soot nanostructure and consequences on loading and regeneration of diesel particulate filters. Combust Flame 2012;159(2):844–53.

[33] Fayad MA, Herreros JM, Martos FJ, Tsolakis A. Role of alternative fuels on particulate matter (PM) characteristics and influence of the diesel oxidation catalyst. Environ Sci Technol 2015;49(19):11967–73. http://dx.doi.org/10.1021/acs.est.5b02447.

[34] Lapuerta M, Sánchez-Valdepeñas J, Barba J, Fernández-Rodríguez D, Andrés JP, García T. Analysis of soot from the use of butanol blends in a Euro 6 diesel engine. Energy & Fuels 2019;33(3):2265–77. http://dx.doi.org/10.1021/acs.energyfuels.8b04083.

[35] Luo J, Zhang Y, Wang J, Zhang Q. Effect of acetone−butanol−ethanol addition to diesel on the soot reactivity. Fuel 2018;226:555–63. http://dx.doi.org/10.1016/j.fuel.2018.04.036.

[36] Zhu L, Xiao Y, Cheung C, Guan C, Huang Z. Combustion, gaseous and particulate emission of a diesel engine fueled with n-pentanol (C5 alcohol) blended with waste cooking oil biodiesel. Appl Therm Eng 2016;102:73–9. http://dx.doi.org/10.1016/j.applthermaleng.2016.03.145.

[37] Pham Q, Park S, Agarwal AK, Park S. Review of dual-fuel combustion in the compression-ignition engine: Spray, combustion, and emission. Energy 2022;123778. http://dx.doi.org/10.1016/j.energy.2022.12377.

[38] Pan M, Wang Y, Wei J, Huang H, Zhou X. Impact of carbon chain length of alcohols on the physicochemical properties and reactivity of exhaust soot. Sci Total Environ 2021;799:149434. http://dx.doi.org/10.1016/j.scitotenv.2021.149434.

[39] Doustdar O. Alternative fuels and aftertreatment systems for low emissions engines (Ph.D. thesis), University of Birmingham; 2019.

[40] Fayad M, Tsolakis A, Fernández-Rodríguez D, Herreros JM, Martos F, Lapuerta M. Manipulating modern diesel engine particulate emission characteristics through butanol fuel blending and fuel injection strategies for efficient diesel oxidation catalysts. Appl Energy 2017;190:490–500. http://dx.doi.org/10.1016/j.apenergy.2016.12.102.

[41] Hamedi M. Advanced thermal management of diesel aftertreatment systems (Ph.D. thesis), University of Birmingham; 2016.

[42] Randolph AL. Methods of processing cylinder-pressure transducer signals to maximize data accuracy. SAE Trans 1990;191–200.

[43] Heywood J. Internal combustion engine fundamentals. McGraw-Hill Education; 1988.

[44] Asad U, Kumar R, Han X, Zheng M. Precise instrumentation of a diesel single-cylinder research engine. Measurement 2011;44(7):1261–78. http://dx.doi.org/10.1016/j.measurement.2011.03.028.

[45] Chen Y, Shah N, Braun A, Huggins FE, Huffman GP. Electron microscopy investigation of carbonaceous particulate matter generated by combustion of fossil fuels. Energy & Fuels 2005;19(4):1644–51. http://dx.doi.org/10.1021/ef049736y.

[46] Ishiguro T, Takatori Y, Akihama K. Microstructure of diesel soot particles probed by electron microscopy: first observation of inner core and outer shell. Combust Flame 1997;108(1–2). http://dx.doi.org/10.1016/S0010-2180(96)00206-4.

[47] Doustdar O, Zeraati-Rezaei S, Herreros JM, Tsolakis A, Dearn KD, Wyszynski ML. Tribological performance of biomass-derived bio-alcohol and bio-ketone fuels. Energies 2021;14(17). http://dx.doi.org/10.3390/en14175331.

[48] Cheng X, Chen L, Hong G, Yan F, Dong S. Modeling study of soot formation and oxidation in DI diesel engine using an improved soot model. Appl Therm Eng 2014;62(2):303–12. http://dx.doi.org/10.1016/j.applthermaleng.2013.09.052.

[49] Frenklach M, Wang H. Detailed modeling of soot particle nucleation and growth. In: Symposium (International) on combustion. 23, (1):Elsevier; 1991, p. 1559–66. http://dx.doi.org/10.1016/S0082-0784(06)80426-1.

[50] Tree DR, Svensson KI. Soot processes in compression ignition engines. Prog Energy Combust Sci 2007;33(3):272–309. http://dx.doi.org/10.1016/j.pecs.2006.03.002.

[51] Haynes BS, Wagner HG. Soot formation. Prog Energy Combust Sci 1981;7(4):229–73. http://dx.doi.org/10.1016/0360-1285(81)90001-0.

[52] Leung KM, Lindstedt RP, Jones W. A simplified reaction mechanism for soot formation in nonpremixed flames. Combust Flame 1991;87(3–4):289–305. http://dx.doi.org/10.1016/0010-2180(91)90114-Q.

[53] Bolla M, Farrace D, Wright YM, Boulouchos K. Modelling of soot formation in a heavy-duty diesel engine with conditional moment closure. Fuel 2014;117:309–25. http://dx.doi.org/10.1016/j.fuel.2013.09.041.

[54] Khawam A, Flanagan DR. Solid-state kinetic models: basics and mathematical fundamentals. J Phys Chem B 2006;110(35):17315–28. http://dx.doi.org/10.1021/jp062746a.

[55] Khawam A, Flanagan DR. Basics and applications of solid-state kinetics: a pharmaceutical perspective. J Pharm Sci 2006;95(3):472–98. http://dx.doi.org/10.1002/jps.20559.

[56] Zaitsev VF, Polyanin AD. Handbook of exact solutions for ordinary differential equations. Chapman and Hall/CRC; 2002, http://dx.doi.org/10.1201/9781420035339.

[57] Lapuerta M, Armas O, Hernández J. Diagnosis of DI Diesel combustion from in-cylinder pressure signal by estimation of mean thermodynamic properties of the gas. Appl Therm Eng 1999;19(5):513–29. http://dx.doi.org/10.1016/S1359-4311(98)00075-1.

[58] Nakamura H, Tanimoto R, Tezuka T, Hasegawa S, Maruta K. Soot formation characteristics and PAH formation process in a micro flow reactor with a controlled temperature profile. Combust Flame 2014;161(2):582–91. http://dx.doi.org/10.1016/j.combustflame.2013.09.004.